Molecular Packing Topology and Interactions to Decipher Mechanical Compliances in Dicyano-Distyrylbenzene Derivatives

Madhubrata Ghora, Ranjit Kumar Manna, Sang Kyu Park, Sangyoon Oh, Sung-Il Kim, Soo Young Park, Johannes Gierschner, Shinto Varghese

Molecular Packing Topology and Interactions to Decipher Mechanical Compliances in Dicyano-distyrylbenzene Derivatives

Madhubrata Ghora, [a] Ranjit Kumar Manna,[a] Sang Kyu Park,[b] Sangyoon Oh,[c] Sung-Il Kim,[c] Soo Young Park,*[c] Johannes Gierschner*[d] and Shinto Varghese*[a]

[a] M. Ghora, R. Manna, Dr. S. Varghese
School of Applied and Interdisciplinary Sciences
Indian Association for the Cultivation of Science
Kolkata 700032, India
E-mail: shinto.varghese@iacs.res.in

[b] Dr. S. K. Park
Institute of Advanced Composite Materials
Korea Institute of Science and Technology
Joellabuk-do, 55324, South Korea

[c] Dr. S. Y. Oh, S.-I. Kim, Prof. S. Y. Park
Department of Materials Science and Engineering,
and Research Institute of Advanced Material
Seoul National University, Seoul, 08826 Republic of Korea
E-mail: parksy@snu.ac.kr

[d] Dr. J. Gierschner
Madrid Institute for Advanced Studies (IMDEA Nanoscience)
Calle Faraday 9, Campus Cantoblanco
Madrid 28049, Spain
E-mail: johannes.gierschner@imdea.org

Abstract: Flexible optoelectronics is the need of the hour as the market moves toward wearable and conformable devices. Crystalline π-conjugated materials offer high performance as active materials compared to their amorphous counterpart, but they are typically brittle. This poses a significant challenge that needs to be overcome to unfold their potential in optoelectronic devices. Unveiling the molecular packing topology and identifying interaction descriptors that can accommodate strain offers essential guiding principles for developing conjugated materials as active components in flexible optoelectronics. The molecular packing and interaction topology of eight crystal systems of dicyano-distyrylbenzene derivatives are investigated. Face-to-face π-stacks in an inclined orientation relative to the bending surface can accommodate expansion and compression with minimal molecular motion from their equilibrium positions. This configuration exhibits good compliance towards mechanical strain, while a similar structure with a criss-cross arrangement capable of distributing applied strain equally in opposite directions enhances the flexibility. Molecular arrangements that cannot reversibly undergo expansion and compression exhibit brittleness. In the isometric CT crystals, the disproportionate strength of the interactions along the bending plane and orthogonal directions makes these materials sustain a moderate bending strain. These results provide an updated explanation for the elastic bending in semiconducting π-conjugated crystals.

Introduction

Organic π-conjugated materials have been in the focus of research for a few decades for applications in optoelectronic devices.[1] While other devices are still awaiting commercialization, the release of organic light emitting diodes in market signifies the success and progress of this research field.[2] Furthermore, this research interest extends to flexible optoelectronics, driven by the belief that organic materials are flexible. While the focus was firstly on polymeric materials,[3] recent attention is shifted towards crystalline molecular materials, in particular due to fewer number of trap sites, detrimental to the optoelectronic response.[4] However, they were relatively unexplored till the recent past, due to difficulties in forming high-quality thin films, as well as for the lack of compliance towards mechanical deformation. The advancement in crystal engineering and understanding of non-covalent interactions provide effective strategies to develop mechanically compliant crystalline molecular materials. [5-7] Alternative approaches by embedding mechanically compliant crystals in polymer matrices which respond to various stimulus were explored for sensing and active materials in optoelectronic devices. [8]

The mechanical flexibility in crystalline materials is of irreversible (plastic) or reversible (elastic); the former is favorable in the drug tabletability while the latter is preferred for flexible optoelectronics applications.[9] In general, structures that exhibit low interaction energy and reduced topological rugosity between planes prefer plasticity due to facilitated interlayer slip.[10] On the other hand, the most widely perceived structural factors responsible for elasticity are a) a molecular arrangement accommodating expansion and compression with minimal molecular motion from the equilibrium position, b) a molecular packing capable of dissipating applied stress equally in opposite directions, c) weak dispersive interactions to avoid interlayer slip as well as to reorganize reversibly on deformation and recovery.[9,11] Specifically, from the molecular arrangement perspective, slipped face-to-face, zig-zag, and crisscross molecular stacks were reported to exhibit elastic bending.[6,12,13] In addition, as we recently highlighted through the crisscross packed pyridine appended thiazolothiazole and its modular co-crystal system, the strength of weak dispersive interactions can have a significant impact on tuning the elastic bending behavior.[14] However, improving mechanical properties of π-conjugated materials with desired optoelectronic functions is challenging because tuning their interactions (π-π, charge transfer, halogen bond and van der Waals (vdW)) entails alteration of their optoelectrical properties simultaneously.[15]

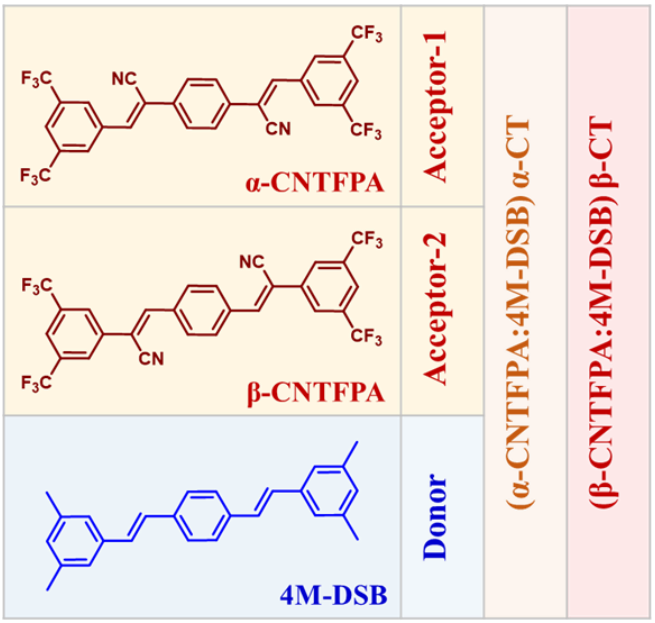

Scheme 1. Chemical structure of the molecules in this article.

Studying crystal systems with similar molecular structures but varying structural and interaction characteristics can provide valuable insights into the effects of these factors on elasticity. The model compounds for the present study are an intriguing class of α-, β-dicyano-distyrylbenzene derivatives with -CF_3 groups in the meta positions of the terminal rings (CNTFPA) and the charge transfer (CT) co-crystals with isometric tetramethyl-distyrylbenzene (4M-DSB), designated as α-CT and β-CT, see Scheme 1. The molecular system constitutes an interesting class of optoelectronic materials, which exhibit high luminescence efficiency, stimulated emission and ambipolar charge transport in the CT crystals.[16] The mechanical properties of these unique molecular crystal systems are of interest for its application to flexible optoelectronic devices. The mechanical properties were however not investigated by now, which is the purpose of the current work. For this, we further extend the existing crystal library [16] by α-CNTFPA polymorphs (and solvated crystals). This allows an unique opportunity to systematically investigate structural and interaction features responsible for elastic bending solely governed by π-π, CT, and vdW interactions.

Results

Molecular Structure and Packing

α-CNTFPA crystallized in two different polymorphic forms with hexagonal and platelet type habit hereafter designated as α-H, and α-P), respectively. The α-H crystallizes in a monoclinic lattice with $P2_1/n$ space group with six molecules in the unit cell (Z = 6), while α -P exhibits an orthorhombic lattice ($Pca2_1$, Z = 4).

In the α-H polymorph, two symmetrically non-equivalent molecules are found in the unit cell, depending on the deviation from planarity. The more planar molecule has an inversion center and deviates from planarity with a torsional angle of 9/6° around the inner/outer (i/o) single bonds in the vinylene unit relative to the central benzene ring (ESI Table-S5). The other molecule lacks an inversion symmetry and having relatively large deviation from planarity on one side with a torsion of 20/23° (i/o) angle and the other vinylene unit with a torsional angle of 6/3° along (i/o) single bonds (ESI Table-S5). A very unique columnar arrangement along the diagonal of the crystallographic 'ac' plane *i.e.*, along (10-1) miller plane (Figure 1a) is observed; this plane constitutes the largest crystal surface as indicated by the specular reflectance X-ray diffraction scans, see ESI Figure S8. Within the columnar arrangement, the molecules sort into a set of three orienting in same direction and then undergo a rotation of 58.5° with respect to the columnar axis. Within the set of three molecules, the nearest neighbors adopted a co-facial slipped stack arrangement with an interplane separation of 3.5 Å (See Table S3, ESI). The slip along the long molecular axis (Δx) is 3.3 Å and along the short axis (Δy) is 0.6 Å (See Table S3, ESI).

In the α-P polymorph, the molecules adopt a nearly planar geometry with a torsion around the inner/outer single bonds of the vinylene units on the either side of the central benzene ring as 5/10° and 10/9°. Nearest neighbors organize in a nearly co-facial manner with a minimal slip along the long molecular axis of 1.9 Å and a relatively larger short axis slip of 2.6 Å. The interplane distance between the nearest dimer is about 3.8 Å as measured between the planes constructed by incorporating all the atoms in the molecule (See ESI-S3). The largest crystalline facet is along (002) Miller indices with the molecules arranged in a slipped face-to-face π-stacks forming a 1D column and crossed edge-to-edge arrangement of the neighboring columns to constitutes an extended crisscross structure as shown in the Figure 1b. The molecules adopted an inclined orientation towards the surface with an angle of 59°; see Table 1.

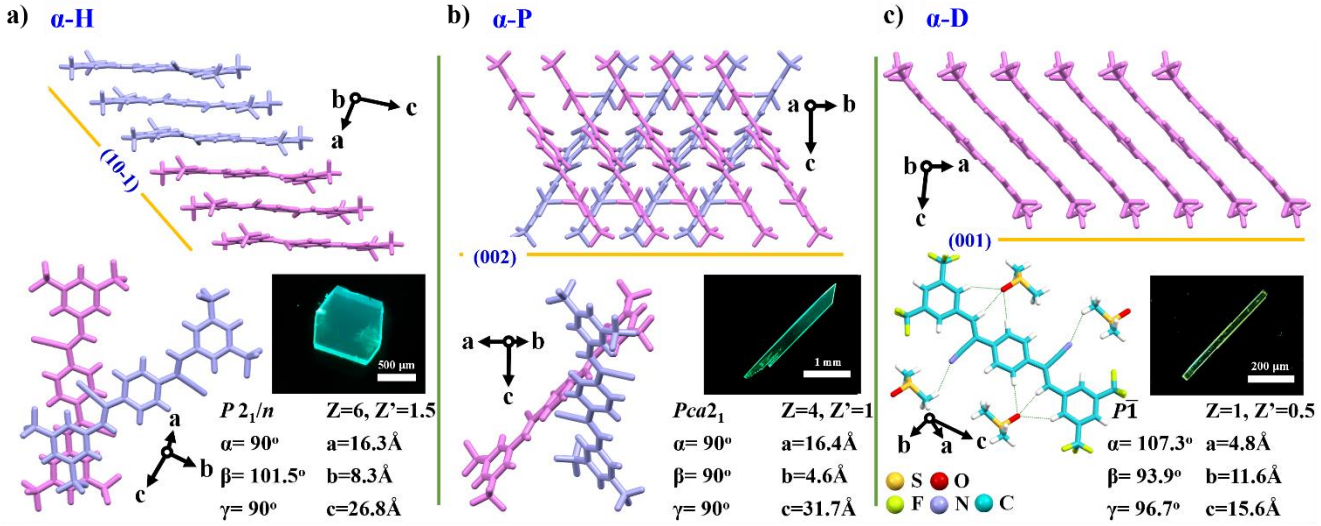

Figure 1. Molecular packing of α-CNTFPA with respect to the largest crystal facet, the fluorescence microscopic images, unit cell parameters and packing within the crystal lattice of a) α- H, b) α- P and c) DMSO solvate crystals (α-D). Two distinct colors (Pink and Blue) are used to represent the stacks if not oriented in the same direction.

Crystallization of α-CNTFPA from DCM/methanol mixture (with a few drops of dimethyl sulfoxide; DMSO) yields solvated crystals with a triclinic crystal lattice ($P\bar{1}$, Z = 1), hereafter designated as α-D. The DMSO molecules interact with α-CNTFPA chromophore through a three centered C-H…O interactions, forming a clearly segregated layers of chromophore and solvent molecules. The α-CNTFPA chromophores arranged in a slipped face-to-face arrangement with an interlayer distance of 3.5 Å. The slip along the long and short molecular axis is 3.27 Å and 0.36 Å, respectively, leaving substantial π-π interactions between the chromophores. The largest crystal surface is along the (001) miller plane as evident from the specular scan (SC)-XRD measurements (See ESI-S8) and the molecular packing with respect to the largest facet of the crystals surface as depicted in the Figure 1c.

Solid state structures of β-CNTFPA chromophore also exist in two monotropic polymorphic forms (i.e. which cannot be interconverted into each other) with distinctly different crystal habit and luminescence behavior (Green and Blue emitting forms). In former reports, a green crystal phase, [16g] as well as a blue and greenish thin film phases were reported. [16b] In the current work, we (re)grew the greenish crystals by slow evaporation from DCM solution, to give crystals elongated hexagonal habit (hereafter β-EH). On the other hand, blue crystals are mostly formed on the sides of the glass container where a faster rate of solvent evaporation occurs from the DCM solution. High quality blue crystals with belt-shaped habit was also developed from a 1,4-Dioxane/DMSO (2:1) solvent mixture by slow evaporation method, which allowed for SC-XRD analysis (hereafter β-B). The crystal structure is very similar to the thin film structure reported earlier. [16b]

The β-EH crystallizes in a monoclinic lattice with $P2_1/c$ space group, essentially reproducing the former results. [16g] The molecules adopt a nearly planar centrosymmetric structure with a torsional angle of 7/6° around the inner/outer (i/o) single bonds in the vinylene unit, respectively. A slipped co-facial arrangement with a 4.3 Å (Δx) slip along the long molecular axis, 2.7 Å (Δy) slip along the short molecular axis and 3.7 Å (See ESI-S3) as the interplanar distance between the nearest dimer structures, leaving moderate π-π interactions between the chromophores. The neighboring stacks oriented in an edge-to-edge fashion with the molecules oriented nearly in the opposite directions constituting a crisscross arrangement with respect to the largest crystalline facet of (100) Miller indices (Figure 2a).

The β-B form crystallizes in a monoclinic lattice with $P21/c$ space group with two molecules in the unit cell. The molecules have a center of symmetric geometry with a twisted conformation of 23°/13° (i/o) dihedral angles along the single bond of the vinylene units. The SC-XRD patterns showed the largest crystal facet is along the (100) miller plane (Figure 2b). A unique 2D layered molecular packing patterns with an intralayer edge-to-edge molecular packing stabilized by fluorophilic interactions followed by a unique interlayer face-to-face cross stack pattern bound by π-stack interactions with adjacent four molecules were observed.

The CNTFPA molecules (both α and β) form CT co-crystals with isometric 4M-DSB through complimentary interactions and electronic features. The details for the preparation of the CT crystals and crystallographic details described elsewhere. [16a,16e] The unit cell parameters, orientation towards the largest crystal facet as well as the micrograph under 365 nm excitation is depicted in Figure 2d, 2e. The isometric donor molecules (4M-DSB) crystallize in a triclinic lattice with $P\bar{1}$ space group with molecules inclined to the largest crystal surface of (001) miller plane (Figure 2c). The 4M-DSB lattice reorient completely to accommodate the donor-acceptor pair and the packing resembles the molecular packing of acceptor (CNTFPA). In both CT crystals, molecules were arranged in a 1D stack of alternating donor-acceptor molecules with nearly same π-π stacking distance of about 3.4 Å. All the molecules adopt a center of symmetric geometry along the barycenter in both CT co-crystals. The 4M-DSB molecules having a planar conformation with a torsional angle of 4/0° (i/o) around the vinylic bond in the α-CT and 1/0º (i/o) in the β -CT crystal lattice. The α-CNTFPA molecules deviate from planarity with a torsional angle of 10/11° around the inner/outer (i/o) single bonds of the vinylene unit in the α-CT

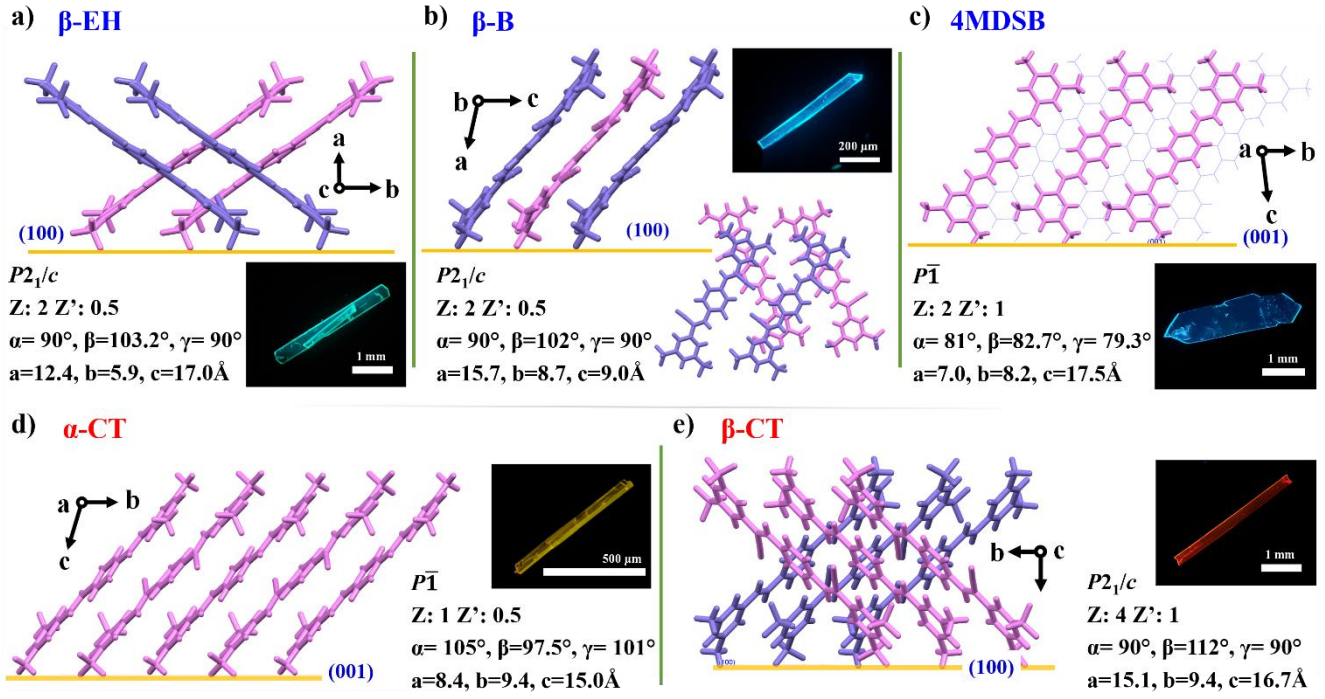

Figure 2. Molecular packing with respect to the largest crystal facet, the fluorescence microscopic images, unit cell parameters and packing within the crystal lattice of β-CNTFPA, i.e. β-EH (a), β-B (b), 4M-DSB c), and of the co-crystals α-CT (d) and β-CT (e). Two distinct colors (Pink and Blue) are used to represent the stacks if not oriented in the same direction.

crystal lattice. A more planar structure of β- CNTFPA molecules with a torsional angle of 5/2° around the inner/outer (i/o) single bonds of the vinylene unit was observed in the β -CT crystal lattice. The XRD pattern in the specular reflection geometry revealed the largest crystal facet is along (001) Miller plane for α-CT and (100) for β-CT (Figure ESI-S8). The 1D slipped stack arrangement of alternating donor-acceptor molecules is inclined to the surface of about 51° in the α-CT and 52° for β-CT. A nearly same slip along the long molecular axis of about 3.3 Å (Δx) between the donor and acceptor molecules were observed for both CT crystals. A short molecular axis slip of 0.2/0.1 Å (Δy) for α-CT and β-CT, respectively. The notable difference in the molecular arrangement in the CT crystals is the orientation of the neighboring stacks. The neighboring 1D stack of alternating DA molecules oriented in same direction in the α-CT while an orthogonal arrangement was observed β-CT crystal lattice (Figure 2d, 2e).

Interaction Topology and Lattice Energies

Nature of intermolecular interactions, i.e. type, directionality as well as energetics dictates the relative positioning of molecules in the crystal lattice and a complete understanding of these factors helps to control crystal growth and physical properties. Hirshfeld surface analysis and pairwise interaction energy calculations were employed to have a complete picture of interaction topology in the present molecular systems. Spackman and co-workers have extended the Hirshfeld electron density partitioning to visualize the intermolecular interactions by considering a 0.5 isosurface weighed function w(r) of the spherical sum of electron density of atoms in a specific molecule (promolecule) to the sum of density of the nearest neighbors (procrystal).[17] The terms d_i and d_e are the distances from the atoms in the interior and from the exterior to the surface, respectively. The normalized contact distance (d_{norm}) was introduced to define the strength of the contacts normalized to the vdW radius of the interacting atoms (equation 1).

$$d_{\text{norm}} = \frac{d_{\text{i}} - r_{\text{i}}^{\text{vdW}}}{r_{\text{i}}^{\text{vdW}}} + \frac{d_{\text{e}} - r_{\text{e}}^{\text{vdW}}}{r_{\text{e}}^{\text{vdW}}} \quad (1)$$

A negative d_{norm} term indicates contacts shorter than vdW radii of separations and positive for contacts greater than vdW separations. The red–white–blue color schemes represent these gradients of interactions i.e. shorter, comparable and longer than the vdW separation, respectively, and thereby distinguish the nature and strength on the interactions. The 2D fingerprint plot generated by plotting d_i against d_e and the interacting atom-to-atom approach provides a percentagewise contribution of these interactions in stabilizing the crystal environment. The Figure 3 depicts the percentagewise contribution of the different interactions stabilizing the crystal and the corresponding HS plot.

The individual atom-atom interaction pattern of these crystal systems showed F···H, F···F, N···H, C···H, H···H, C···C as the major contributors for stabilizing the crystal lattice and all other minor contributions lower than 7% percentage in any of the systems combined under the label of other interactions. A complete detail of the interactions and the method of calculation can be seen in the supporting information. The major interactions in different polymorphs of the acceptor molecules, i.e. both α- and β-CNTFPA are dominated by F···F and F···H interactions. These interactions contribute more than 50% of the overall interactions and is key in stabilizing the packing. In the solvated crystal (α-D) these combined interactions contribute about 44% and are crucial. The O···H interactions, which stabilizes the DMSO-CNTFPA interactions, amount 7%. In the 4M-DSB donor crystal lattice, due to the local edge-to-face packing of the aromatic units, C···H and H···H interactions are dominant in the overall intermolecular interactions. In both CT crystals, the interactions types are very similar, where F···H and H···H interactions contribute nearly 60% of the total interactions. The major difference in the interaction

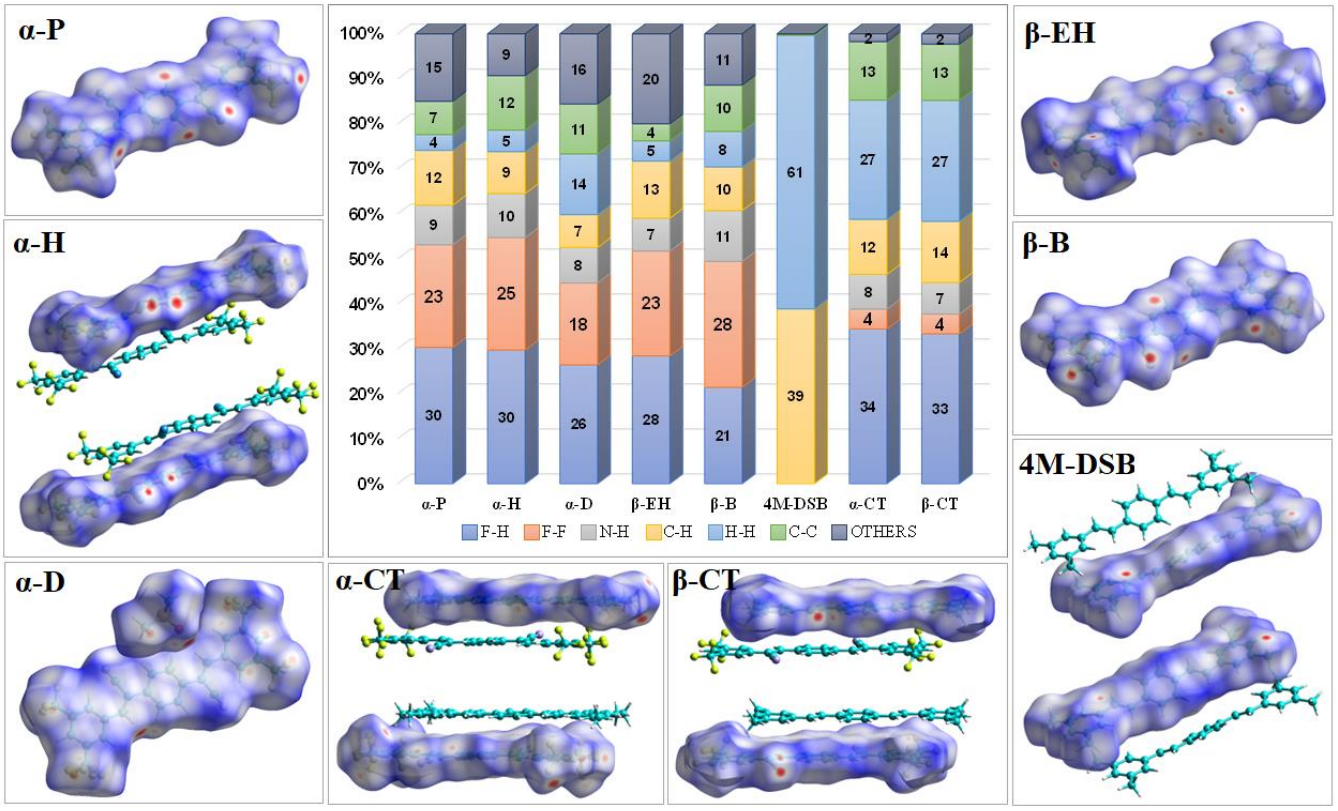

Figure 3. Hirschfeld isosurface representations of the systems under investigation; the percentagewise contribution of the interactions in the crystals is given, considering all unsymmetrical molecules separately, and weighted to the number of atoms in the molecules.

pattern compared to the acceptor molecules alone are seen in the considerable reduction of F···F interactions (~20% to 4%). An enhancement in C···C interaction to 13% is observed in both CT crystals, due to the mixed D-A packing.

Lattice energies

The lattice energies (LE) were calculated from the total interaction energy quantified by the summation of pairwise interaction energy of a central molecule to the neighboring molecules with a cutoff center-to-center distance of 20Å and scaled to the number of same kind of individual molecules and their stoichiometry. [18] Individual lattice energies were calculated and averaged for the crystal lattice with more than one unique molecule per unit cell (Z' > 1). For co-crystals and solvated crystal, individual lattice energies were calculated for different co-formers and summed up to get the total interaction energy and scaled to the co-former units to determine the lattice energy. The pairwise interaction energies were calculated using B3LYP-D3 functional with 6-31G(d,p) basis set as implemented in the Crystal Explorer 17.5 program. The total interaction energy and the electrostatic, polarization, dispersion, and exchange–repulsion components of the molecular systems under consideration are depicted in Figure 4a.

Both polymorphs of the α-CNTFPA derivative (α-P and α-H) have lattice energies of -235.1 and -232.6 kJ/mol, respectively. The lattice energy difference between these forms is ΔE_{Latt} = 2.5 kJ/mol, with α-P as the more stable form. While in the polymorphs of the β-CNTFPA, β-B and β-EH having the energies -228.6 and -225.4 kJ/mol, respectively, thus giving ΔE_{Latt} = 3.2 kJ/mol. Hereby, mainly dispersion contributes towards the total interaction energy, due to the strong π-π interactions between the planar π-conjugated cores. The total energy of the 4M-DSB is lowest among the crystals investigated, with 185.1kJ/mol, despite of the planar π-conjugated core; this is due to the absence of fluorophilic interactions that exist in the alpha and beta forms. In the case of α-D, electrostatic interactions between the α-CNTFPA core and the DMSO molecules give rise to a total interaction energy of -308.9kJ/mol which results in a lattice energy of -103 kJ/mol; this is substantially lower than that of the α-CNTFPA polymorphs.

The total interaction energies of the isometric CT crystals (α- and β-CT) are substantially higher than the polymorphs of the acceptors alone (α-P, -H, and β-B, -EH), as well as the solvated crystal (α-D). The total interaction energies of α-CT and β-CT crystals are -400.6 kJ/mol and -397.7 kJ/mol, respectively, with dispersion as the major component while having a reasonable contribution from the electrostatic interaction. The total interaction energies were scale to the co-former units to get a lattice energy of 200.3 kJ/mol and 198.5 kJ/mol for α-CT and β-CT, respectively. The CT crystals are thus thermodynamically less stable compared to the acceptor crystals. However, the substantially high total interaction energy allows the formation of these crystals from the respective components. The calculated values are more or less in agreement with the LE calculated from the Gavezzotti method. (See SI).

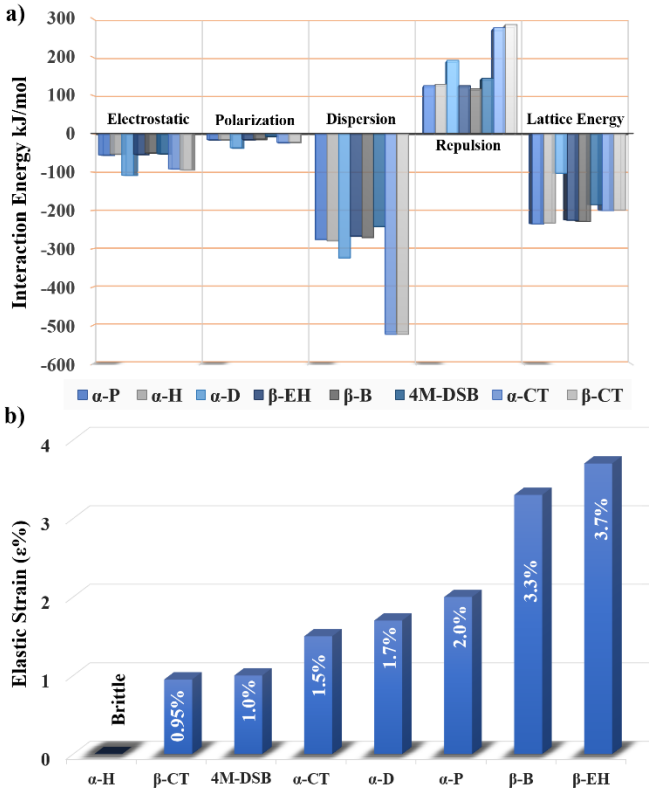

Figure 4. a) Contributions of electrostatic, polarization, dispersion, and repulsion interactions to the lattice energies and b) the percentage of bending strain calculated by the Euler-Bernoulli equation for the molecules under investigations.

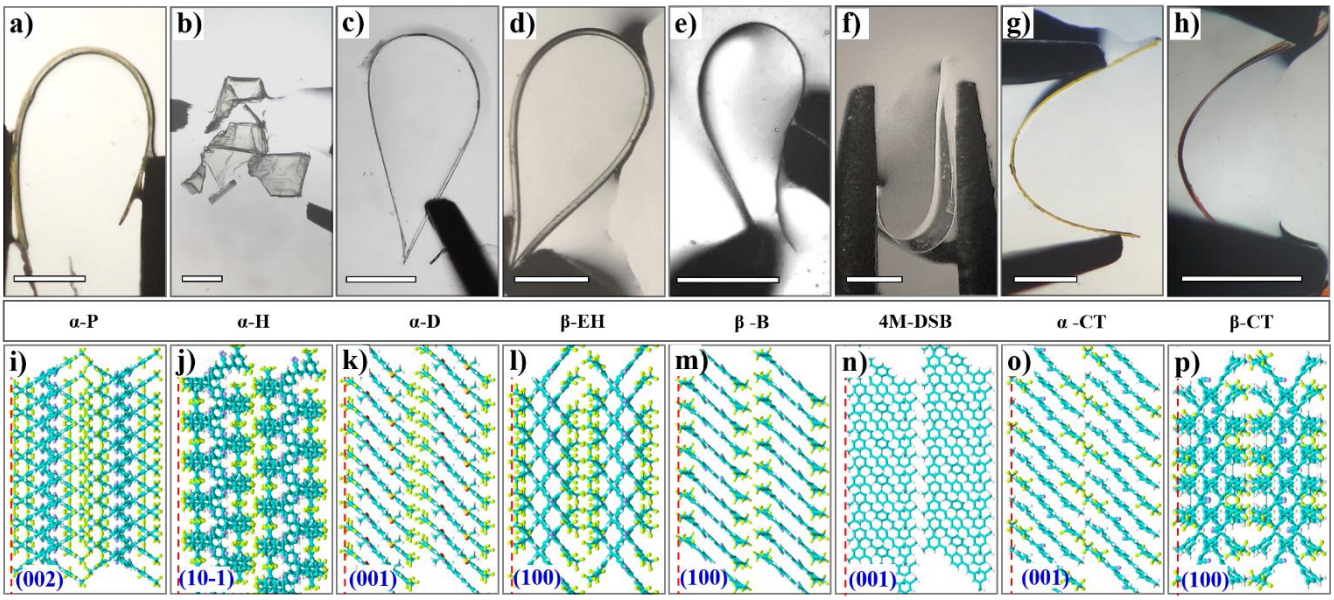

Figure 5. Representative images of the polymorphs, solvate crystals and isometric CT crystals on applying bending strain: (a) α-P, b) α-H, c) α-D, d) β-EH, e) β-B, f) 4M-DSB, g) α-CT, h) β-CT; the scale bar (white line) is 500 μm. The corresponding molecular packing with respect to the bending plane are shown below (i–p).

The donor-acceptor interactions along with the complementarity in the structural factors favor the electrostatic as well as the dispersion components and contribute towards the higher lattice energies.

Mechanical Properties

Mechanical compliances towards bending strain in these crystal systems were examined by applying mechanical stress at both ends of the crystals to form a loop by means of a pair of forceps. Except for α-H crystals, all the other crystal systems have certain degree of compliances towards mechanical stress and straitened upon the withdrawal of the force. The degree of flexibility varies with different crystal systems, and are quantified in terms of percentage of sustainable mechanical strain from the radius of curvature (r) of the bend and the thickness (t) of the crystal using a simple relationship (ε (%)=t/2r×100). The percentage of strain that the crystals can sustain is highest in the β-EH form (3.7%) and lowest for β-CT with 1.0%, while α-H crystals are brittle in nature. The percentage of sustainable strain upon bending for these crystal systems are depicted in Figure 4b and are in the range of brittle, moderate to good compared to the molecular systems investigated in literature. [6,12,19] Nanoindentation was not attempted on these solution-grown bulk crystals as the single-point indentation measurements are not ideal for such crystals as they overlook the defect densities. Additionally, the anisotropic mechanical response, which is inherently tensorial and face dependent, further complicates the scenario in low-symmetry organic crystals especially crystals with an elastic strain above 1% is not reliable. [12,20]

Discussions

The crystals presented here (CNTFPA polymorphs, solvate and isometric CT crystals) constitutes a unique class of materials with linear π-conjugated distyrylbenzene (DSB) backbone, where the molecular packing is dictated by weak dispersive interactions, relevant for active materials in optoelectronic devices. The waveguide properties and fluorescence changes upon nanoscopic structural change during mechanical bending of a dicyano-distyrylbenzene derivative were reported, recently. [9d] The aspect ratios of all these molecules under investigations are nearly isometric and the molecular packing governed mostly by π-π, C-H···π, F···F, CT interactions. The observed varying degree of bending strain in these crystals gives us an opportunity to understand and quantify various structural, interaction and packing factors that contribute towards mechanical compliances. From bending studies, it is evident that the crystals other than that of α-H exhibit a good to reasonable degree of mechanical compliances towards bending strain and relaxes to the original form on the removal of the strain. Elastic bending requires the reversible expansion and contraction of the outer and inner surface with minimal slippage between the planes. The intralayer molecular packing with zig-zag, crisscross, and slipped π-stack

Table 1. Crystal features and intermolecular arrangements of the compounds under study.

Packing / Properties	Acceptors					Donor	Isometric CT	
	α-CNTFPA			β-CNTFPA		4M- DSB	α-CT	β-CT
	α-P	α-H	α-D	β-EH	β-B			
Crystal Habit	Thin Plates	Thick Hexagon	Thin Needles	Elongated Hexagonal Plates	Long Belt	Thin Plates	Long Needles	Elongated Hexagonal platelets
Crystal Surface*[a]	(002)	(10-1)	(001)	(100)	(100)	(001)	(001)	(100)
Inclination [b]	59°	59.4°	47°	37°	54°	55-57°	51°	52.5°
Surface Layer (+Separation/ -Interdigitation)[c]	-0.21	+0.21	-0.45	+0.09	+0.63	+0.38	+0.04	-0.09
Slip Planes (Separation Distance)	No	10-1 (0.21)	10-3 (0.21)	100 (0.09)	100 (0.63)	201 (1.08), 001 (0.38)	001 (0.04)	No
Orthogonal to bending surface	No	No	No	No	No	Yes	Yes	No
Void Space[d]	5.1%	7.0%	15.3%	10.7%	13.9%	12.9%	14.5%	11.8%
Displacement in Dimers (Δx,Δy,Δz)[e]	1.91, 2.56, 3.22	3.24, 0.63, 3.48	3.26, 0.36, 3.48	4.24, 2.66, 3.10	4.47, 2.64, 3.57	1.67, 0.92, 4.49	3.26, 0.19, 3.37	3.27, 0.10, 3.35
Intralayer Stacking [f]	Criss-cross	Parallel/ Crossed π-Stack	Parallel	Criss-cross	Parallel/ Crossed π-Stack	Parallel	Parallel	Criss-cross
Interlayer Stacking [g]	Zig-Zag	Parallel/ Opposite	Parallel	Zig-zag	Parallel	Parallel	Parallel	Parallel
Mechanical Compliances (ε/%)	Flexible (~2.0%)	Brittle	Flexible (~1.7%)	Flexible (~3.7%)	Flexible (~3.3%)	Flexible (~1.0%)	Flexible (~1.5%)	Flexible (~1.0%)

[a] Major crystal facet determined from specular scanning X-ray diffraction, and in concurrence with BFDH morphology prediction (see also Figure 5). [b] Angle of inclination of molecular long axis, with respect to the major crystal facet. [c] (-) value denotes that layers are interdigitated. and (+) value indicate as separated layers (in Å).[10c] [d] Void space determined by using a probe of radius 0.5 Å and grid spacing of 0.5 Å [e] Estimated by preparing centroid of molecules in the dimer; displacement along the long molecular axis is denoted by Δx, along short molecular axis Δy, and π-stacking direction is Δz (see SI for more details). [f] Layer considered along the short molecular axis. [g] Layer considered along long molecular axis.

arrangements with sufficient void space to accommodate expansion/contraction enables elastic bending. The zig-zag molecular packing perpendicular to the bending plane and the cross-stacks extending along the bending plane can accommodate the expansion and compression by minimal movements from the equilibrium positions in opposite directions and counterbalances the strain. The isotropic distribution of strain helps to avoid surpassing the linear Hook's law regime in the stress-strain plot to have plastic deformation. The slipped π-stack structure with an inclined molecular orientation towards the bend plane can also accommodate the strain to a larger extend without deforming into plasticity or rupture. This is mainly due to the minimal molecular motion required for bending and the unidirectionality in the distribution of the stress on the slipped molecular arrangements as well as, which is very much relevant to the linear π-conjugated molecules as demonstrated by Hayashi and co-workers.[6] However, the counterbalance of the strain to the opposite direction is lacking and expected to have less sustainable towards bending strain.

The strength of the interaction as well as the topology of the interaction which facilitate the isotropic distribution of strain also matters, as this enables to accommodate reversible stretching and compression on bending/relaxation process. Slip planes, as derived from the rugosity point of view, play a major role in determining the mechanical compliance towards bending strain. A large number of slip planes in different orientations favor the molecules' slide passing each other to induce a permanent deformation. The slip planes along the bend plane enhance the plastic bending, while the slip planes perpendicular to the bending surface are reported to be beneficial for the elastic bending.[10c] When slip planes are oriented parallel to the bending plane, dislocations can move easily, allowing the material to bend plastically, while in the perpendicular direction allows the volume accommodation required for the stretching/compression process. Table 1 summarizes the overview of packing descriptors to decipher the mechanical compliances in these molecular crystal systems based on the above-mentioned general perceptions on mechanical compliances.

Both α-P and β-EH polymorphs exhibit a (2D) crisscross molecular packing along the bending plane and the zig-zag orientation of molecules orthogonal to the bending surface and thus favors the elastic bending. The multiple fluorophilic interaction between the CF_3 groups are present in both of the derivatives, reinforcing the structural integrity on bending and relaxation. These interactions constitute an -0.21 Å interdigitated arrangement of molecules orthogonal to the bending plane in the α-P while a slip plane (100) of + 0.09 Å separation in β-EH. For the former case, the lesser degree of inclination towards the bending surface (59^o) and tightly packed chromophores with a minimal void space of 5.1% might be the reasons for the moderate sustainability towards the bending strain of 2.0%. While all the other factors along with the inclination of 37^o towards the bending surface and void space of 10% are in favor of β-EH to have the highest bending strain (3.7%) observed in these derivatives.

Both of the α-H and β-B derivatives exhibit a 1D crossed π-stacking arrangement along the bending surface with an inclined orientation of molecules (59^0 and 54^0) with respect to the bending plane (10-1) and (100), respectively. Slip planes along the bending surface with a three times higher separation distance (+0.63Å) was observed in the β-B packing compared to the α-H derivative with a separation of (+0.21Å). This along with the higher void spacing favors the β-B packing for a higher bending strain of 3%. However, in α-H, unique intralayer packing with three molecules oriented in the same direction and the next set of three oriented in the opposite direction constitutes a crossed arrangement along the (10-1) bending surface (ESI S17). Due to the weaker face-to-face cross-stacking interactions, which exist and repeats after every group of three strongly bound π-stacked trios, the balanced distribution of the strain in the crystal along the bending plane is disrupted. In the orthogonal direction, within these trios a pair of molecules oriented opposite direction and the next molecules align parallel to the upper layer further disrupts the balanced distribution of the bending strain and resulted in the rupture of the crystal habit on applying bending strain.

In α-D and 4M-DSB, crossed packing arrangements of molecules are absent; rather an inclined orientation of the molecules toward the bending surface are observed. A planar face-to-face π-stacking aggregates with a reasonable slip along the long molecular axis was observed along the bending surface in the α-D. The inclined packing with the face-to-face π-stacking interactions along the bending plane is capable of sustain a moderate bending strain of 1.7%. The strong dispersive π-stacking interaction between the aromatic cores and the electrostatic interactions between chromophore-DMSO molecules favors the bending. A compromised π-stacks were observed in the 4M-DSB derivative with a reasonable slip along the short molecular axis and the CH-π interactions in the central benzene rings distort the molecules in the center. However, the existing weak π-stacking interactions are orthogonal to the applied stress; therefore, the observed packing is not in favor of sustaining a high bending strain, resulting in a bending percentage of 1%.

A face-to-face π-stacked (CT) aggregates with an inclined orientation exist in the α-CT cocrystal, while an edge-to-edge cross-stacking aggregation along the bending plane was observed in the β-CT cocrystal. The molecular packing descriptors are favorable for a higher bending strain. However, these isometric CT crystals exhibit a moderate bending strain of 1.5% and 1.0% for α-CT and β-CT, respectively. Both crystals are characterized by strong CT interactions along the bend plane while a weak interlay interaction between the layers orthogonal to the bending plane are found. In the β-CT there is literally no interactions between the layers in orthogonal directions, while a single F-F interaction is present from a short contact, i.e. lesser than the Van der Waal's distance between the atoms. This interaction topology makes the structure more vulnerable to slippage, and results in the rupture on applied stress after a moderate strain.

Conclusion

We have demonstrated mechanical compliances in a series of isometric distyrylbenzene polymorphs, solvate and CT crystals. We have shown a series of arrangements that can accommodate various degrees of mechanical strain on bending deformation, and can be used as a directive for these systems to decipher the mechanical compliances. The molecular packing features responsible for the dissipation of applied stress with minimal structural deviation from its equilibrium positions is primarily responsible for the elastic bending in these crystals systems. The intralayer face-to-face slipped π-stacks with the molecules inclined towards the bend plane can accommodate the stretching and relaxation upon bending/straightening without large amplitude movement, and the π-stacks binds the molecules from slipping apart. The intralayer crisscross orientation of the slipped π-stacks is more accommodative towards the applied strain by dissipating the stress equally in opposite directions. Interlayer interactions are shown to take a pivotal role in accommodating the compression/expansion upon bending and relaxation and are essential for achieving mechanical compliances. Our investigations are thus providing guiding principles for the development of linear π-conjugated molecules/systems with a certain degree of mechanical compliance without compromising the functional performance, that can be utilized for adaptable optoelectronic devices.

Acknowledgements

The work at IACS was supported under the SERB project (CRG/2022/008007), Technical Research Center project second phase at IACS and institutional funds are gratefully acknowledged. The work in Madrid was supported by the Spanish Ministerio de Ciencia, Innovación (MICIN-FEDER) project PID2022-138222NB-C21, by the Severo Ochoa program for Centers of Excellence in R&D of the MICIN (CEX2020-001039-S) and by the Campus of International Excellence (CEI) UAM+CSIC. The work in KIST was supported by the Basic Science Research Program through the National Research Foundation of Korea (NRF) funded by the Ministry of Education (2022R1C1C1005241) and the Korea Institute of Science and Technology (KIST) Institutional Program.

Deposition Numbers 2339728-2339731 contains the supplementary crystallographic data for this paper. These data are provided free of charge by the joint Cambridge Crystallographic Data Centre and Fachinformationszentrum Karlsruhe.

Keywords: Mechanical Compliance• Intermolecular interactions • Molecular Packing• Polymorphs• Charge Transfer Crystals.

[1] (a) S. R. Forrest, *Nature* **2004**, *428*, 911–918. (b) O. Ostroverkhova, *Chem. Rev.* **2016**, *116*, 13279–13412. (c) F. Yang, S. Cheng, X. Zhang, X. Ren, R. Li, H. Dong, W. Hu, *Adv. Mater.* **2018**, *30*, 1702415.

[2] (a) Y. Liu, C. Li, Z. Ren, S. Yan, M. R. Bryce, *Nat. Rev. Mater.* **2018**, *3*, 18020. (b) H. Sirringhaus, *Adv. Mater.* **2014**, *26*, 1319–1335. (c) Z. Qin, H. Gao, H. Dong, W. Hu, *Adv. Mater.* **2021**, *33*, 2007149.

[3] (a) K. Liu, B. Ouyang, X. Guo, Y. Guo, Y. Liu, *npj Flex. Electron.* **2022**, *6*, 1. (b) S. E. Root, S. Savagatrup, A. D. Printz, D. Rodriquez, D. J. Lipomi, *Chem. Rev.* **2017**, *117*, 6467–6499.

[4] (a) B. Fraboni, A. Fraleoni-Morgera, Y. Geerts, A. Morpurgo, V. Podzorov, *Adv. Funct. Mater.* **2016**, *26*, 2229–2232. (b) Y. Wang, L. Sun, C. Wang, F. Yang, X. Ren, X. Zhang, H. Dong, W. Hu, *Chem. Soc. Rev.* **2019**, *48*, 1492–1530.

[5] (a) G. R. Desiraju, *J. Am. Chem. Soc.* **2013**, *135*, 9952–9967. (b) P. Naumov, S. Chizhik, M. K. Panda, N. K. Nath, E. Boldyreva, *Chem. Rev.* **2015**, *115*, 12440–12490. (c) E. Ahmed, D. P. Karothu, P. Naumov, *Angew. Chem., Int. Ed.* **2018**, *57*, 8837–8846. (d) S. Das, A. Mondal, C. M. Reddy, *Chem. Soc. Rev.* **2020**, *49*, 8878–8896.

[6] (a) S. Hayashi, S. ya Yamamoto, D. Takeuchi, Y. Ie, K. Takagi, *Angew. Chem., Int. Ed.* **2018**, *57*, 17002–17008. (b) S. Hayashi, T. Koizumi, *Chem. Eur. J.* **2018**, *24*, 8507–8512. (c) S. Hayashi, *Symmetry (Basel).* **2020**, *12*, 2022. d) S. Hayashi, *Bull. Chem. Soc. Jpn.* **2022**, *95*, 721–727. e) S. Hayashi, T. Koizumi, *Angew. Chem., Int. Ed.* **2016**, *55*, 2701–2704.

[7] (a) W. M. Awad, D. W. Davies, D. Kitagawa, J. Mahmoud Halabi, M. B. Al-Handawi, I. Tahir, F. Tong, G. Campillo-Alvarado, A. G. Shtukenberg, T. Alkhidir, Y. Hagiwara, M. Almehairbi, L. Lan, S. Hasebe, D. P. Karothu, S. Mohamed, H. Koshima, S. Kobatake, Y. Diao, R. Chandrasekar, H. Zhang, C. C. Sun, C. Bardeen, R. O. Al-Kaysi, B. Kahr, P. Naumov, *Chem. Soc. Rev.* **2023**, *52*, 3098–3169. (b) P. Naumov, D. P. Karothu, E. Ahmed, L. Catalano, P. Commins, J. M. Halabi, M. B. Al-Handawi, L. Li, J. Am. Chem. Soc. 2020, 142, 31, 13256–13272.

[8] a) L. Lan, X. Yang, B. Tang, X. Yu, X. Liu, L. Li, P. Naumov, H. Zhang, *Angew. Chem., Int. Ed.* **2022**, *61*, e202200196. b) X. Yang, L. Lan, L. Li, X. Liu, P. Naumov, H. Zhang, *Nat. Commun.* **2022**, *13*, 2322. c) X. Yang, L. Lan, L. Li, J. Yu, X. Liu, Y. Tao, Q. H. Yang, P. Naumov, H. Zhang, *Nat. Commun.* **2023**, *14*, 3627. d) X. Yang, L. Lan, X. Pan, Q. Di, X. Liu, L. Li, P. Naumov, H. Zhang, *Nat. Commun.* **2023**, *14*, 2287. e) S. Tang, K. Ye, P. Commins, L. Li, P. Naumov, H. Zhang, *Adv. Opt. Mater.* **2023**, *11*, 2200627.

[9] (a) S. Hu, M. K. Mishra, C. C. Sun, *Chem. Mater.* **2019**, *31*, 3818–3822. (b) S. Karki, T. Friščić, L. Fabián, P. R. Laity, G. M. Day, W. Jones, *Adv. Mater.* **2009**, *21*, 3905–3909. (c) T. Matsuo, K. Ikeda, S. Hayashi, *Aggregate* **2023**, e378. (d) S. Zhao, H. Yamagishi, O. Oki, Y. Ihara, N. Ichiji, A. Kubo, S. Hayashi, Y. Yamamoto, *Adv. Opt. Mater.* **2022**, *10*, 2101808.

[10] (a) C. C. Sun, Y.-H. Kiang, *J. Pharm. Sci.* **2008**, *97*, 3456–3461. (b) C. Wang, C. C. Sun, *Cryst. Growth Des.* **2018**, *18*, 1909–1916. (c) M. J. Bryant, A. G. P. Maloney, R. A. Sykes, *CrystEngComm* **2018**, *20*, 2698–2704.

[11] (a) R. Devarapalli, S. B. Kadambi, C. T. Chen, G. R. Krishna, B. R. Kammari, M. J. Buehler, U. Ramamurty, C. Malla Reddy, *Chem. Mater.* **2019**, *31*, 1391–1402. (b) A. Worthy, A. Grosjean, M. C. Pfrunder, Y. Xu, C. Yan, G. Edwards, J. K. Clegg, J. C. McMurtrie, *Nat. Chem.* **2018**, *10*, 65–69. (c) H. Liu, Z. Lu, B. Tang, C. Qu, Z. Zhang, H. Zhang, *Angew. Chem., Int. Ed.* **2020**, *59*, 12944–12950. (d) Z. Lu, Y. Zhang, H. Liu, K. Ye, W. Liu, H. Zhang, *Angew. Chem., Int. Ed.* **2020**, *59*, 4299–4303. e) A. J. Thompson, J. R. Price, J. C. McMurtrie, J. K. Clegg, *Nat. Commun.* **2021**, *12*, 5983. f) A. J. Thompson, A. I. Chamorro Orué, A. J. Nair, J. R. Price, J. McMurtrie, J. K. Clegg, *Chem. Soc. Rev.* **2021**, *50*, 11725–11740.

[12] S. Ghosh, M. K. Mishra, S. B. Kadambi, U. Ramamurty, G. R. Desiraju, *Angew. Chem., Int. Ed.* **2015**, *54*, 2674–2678.

[13] (a) H. Liu, K. Ye, Z. Zhang, H. Zhang, *Angew. Chem., Int. Ed.* **2019**, *58*, 19081–19086. (b) S. Hayashi, A. Asano, N. Kamiya, Y. Yokomori, T. Maeda, T. Koizumi, *Sci. Rep.* **2017**, *7*, 9453.

[14] M. Ghora, P. Majumdar, M. Anas, S. Varghese, *Chem. Eur. J.* **2020**, *26*, 14488–14495.

[15] (a) A. L. Briseno, R. J. Tseng, M. M. Ling, E. H. L. Falcao, Y. Yang, F. Wudl, Z. Bao, *Adv. Mater.* **2006**, *18*, 2320–2324. (b) Y. An, H. Wang, *J. Mater. Sci. Mater. Electron.* **2023**, *34*, 665.

[16] (a) S. Oh, S. K. Park, B. H. Jhun, J. C. Roldao, J. H. Kim, M. W. Choi, C. H. Ryoo, S. Jung, N. Demitri, R. Fischer, I. E. Serdiuk, R. Resel, J. Gierschner, S. Y. Park, *J. Phys. Chem. C* **2020**, *124*, 20377–20387. (b) M. J. Aliaga-Gosalvez, N. Demitri, M. Dohr, J. C. Roldao, S. K. Park, S. Oh, S. Varghese, S. Y. Park, Y. Olivier, B. Milián-Medina, R. Resel, J. Gierschner, *Adv. Opt. Mater.* **2019**, *7*, 1900749. (c) S. Varghese, S. K. Park, S. Casado, R. Resel, R. Wannemacher, L. Lüer, S. Y. Park, J. Gierschner, *Adv. Funct. Mater.* **2016**, *26*, 2349–2356. (d) M. Wykes, S. K. Park, S. Bhattacharyya, S. Varghese, J. E. Kwon, D. R. Whang, I. Cho, R. Wannemacher, L. Lüer, S. Y. Park, J. Gierschner, *J. Phys. Chem. Lett.* **2015**, *6*, 3682–3687. (e) S. K. Park, S. Varghese, J. H. Kim, S. J. Yoon, O. K. Kwon, B. K. An, J. Gierschner, S. Y. Park, *J. Am. Chem. Soc.* **2013**, *135*, 4757–4764. (f) S. Varghese, S. K. Park, S. Casado, R. C. Fischer, R. Resel, B. Milián-Medina, R. Wannemacher, S. Y. Park, J. Gierschner, *J. Phys. Chem. Lett.* **2013**, *4*, 1597–1602. (g) S. K. Park, J. H. Kim, S. J. Yoon, O. K. Kwon, B. K. An, S. Y. Park, *Chem. Mater.* **2012**, *24*, 3263–3268. (h) S. K. Park, J. H. Kim, T. Ohto, R. Yamada, A. O. F. Jones, D. R. Whang, I. Cho, S. Oh, S. H. Hong, J. E. Kwon, J. H. Kim, Y. Olivier, R. Fischer, R. Resel, J. Gierschner, H. Tada, S. Y. Park, *Adv. Mater.* **2017**, *29*, 1701346.

[17] (a) J. J. McKinnon, D. Jayatilaka, M. A. Spackman, *Chem. Commun.* **2007**, 3814–3816. (b) M. J. Turner, S. P. Thomas, M. W. Shi, D. Jayatilaka, M. A. Spackman, *Chem. Commun.* **2015**, *51*, 3735–3738. (c) S. P. Thomas, M. W. Shi, G. A. Koutsantonis, D. Jayatilaka, A. J. Edwards, M. A. Spackman, *Angew. Chem., Int. Ed.* **2017**, *56*, 8468–8472. (d) P. R. Spackman, M. J. Turner, J. J. McKinnon, S. K. Wolff, D. J. Grimwood, D. Jayatilaka, M. A. Spackman, *J. Appl. Crystallogr.* **2021**, *54*, 1006–1011.

[18] (a) M. A. Spackman, *CrystEngComm* **2018**, *20*, 5340–5347. (b) S. P. Thomas, M. A. Spackman, *Aust. J. Chem.* **2018**, *71*, 279–284.

[19] (a) M. Đaković, M. Borovina, M. Pisačić, C. B. Aakeröy, Ž. Soldin, B. M. Kukovec, I. Kodrin, *Angew. Chem., Int. Ed.* **2018**, *57*, 14801–14805. (b) M. K. Mishra, C. C. Sun, *Cryst. Growth Des.* **2020**, *20*, 4764–4769.

[20] S. Varughese, M. S. R. N. Kiran, U. Ramamurty, G. R. Desiraju, *Angew. Chemie Int. Ed.* **2013**, *52*, 2701–2712.

Entry for the Table of Contents

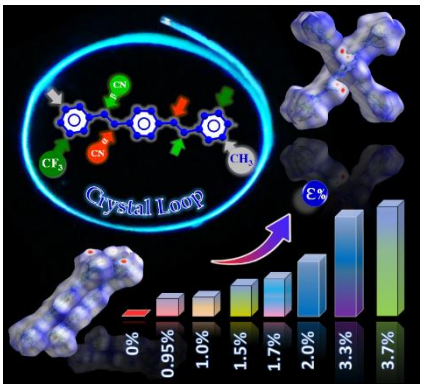

The molecular packing and interaction topology of eight crystal systems, including polymorphs, solvate crystal, and isometric charge transfer crystals of dicyano-distyrylbenzene derivatives with similar molecular structures but varying structural and interaction characteristics were investigated in detail to explore the key molecular arrangements necessary for mechanical compliance. The results provide an updated explanation for the elastic bending observed in semiconducting π-conjugated crystals.